Research Article

Towards High Solar Contribution in Hybrid CSP-Combined Cycle Gas Turbine Plants

Antonio Rovira [ID],[1] Rubén Barbero [ID],[1] Guillermo Ortega [ID],[2] Antonio Subires [ID],[1] and Marta Muñoz [ID][1]

[1]*National University of Distance Education, UNED, Spain*
[2]*School of Engineering, University of Huelva, UHU, Spain*

Correspondence should be addressed to Antonio Rovira; rovira@ind.uned.es

This paper proposes and analyses several configurations for hybridising concentrating solar power (CSP) plants with combined cycle gas turbines (CCGT). The objective is to increase the solar contribution to a large extent, much higher than those obtained in integrated solar combined cycles but maintaining synergies, which are usually lost when increasing the solar share. For that, two thermal energy management systems are introduced at different temperature levels. First, a configuration with only the low-temperature system is proposed. Then, an enhanced configuration with the low- and high-temperature systems is conceived. These configurations are compared to reference CSP and CCGT state-of-the-art plants. The analyses include different strategies of operation and two sizes for the thermal energy storage system. The results show that the first proposed configuration introduces some synergies but cannot improve the performance of the reference CSP and CCGT working separately, due to an issue with the solar dumping on days with high solar irradiation. The enhanced configuration overcomes this problem and maintains the synergies, leading to an improvement from both the thermodynamic and economic points of view, increasing the solar contribution and decreasing the levelized cost of energy over the reference plants.

1. Introduction

CSP provides dispatchable electricity from a nondispatchable renewable source, such as solar energy. This not only ensures sustainability but also enables CSP plants to work at both baseload or peak scenarios while stabilizing and increasing the reliability of the electricity grid, which is particularly required when the penetration of renewable energies is high ([1, 2]).

CSP is usually deployed through standalone power plants, but it can be hybridized with other power plants and resources, such as gas-fired or biogas power plants. In this regard, integrated solar combined cycles (ISCC) stand as an interesting technology, integrating CSP into a combined cycle gas turbine (CCGT) plant [3]. The technical literature shows that there is a wide consensus regarding of the synergies between CCGT and CSP [4–6]. The main reason to find synergies is that the production of conventional CCGT plants decreases on the days of high solar radiation due to the high ambient temperature, which is when the solar field of the CSP performs best. Nevertheless, they go beyond. Indeed, there are multiple points where the solar energy can be supplied [7–10] and many available CSP technologies that open a wide optimisation window [11, 12] to make the integrated plant more efficient than the CCGT and CSP plants working separately.

However, ISCCs have two main weaknesses. On the one hand, to reach good synergies, the nominal solar contribution over the total nominal production is small [6, 12, 13]. For example, Al-Abdaliya ISCC plant [14] includes $60\,MW_{th}$ in a $280\,MW_e$ CCGT; Khandelwal et al. [5] consider $15\,MW_{th}$ into a $320\,MW_e$ one; Duan et al. [15] consider

$40\,\mathrm{MW_{th}}$ within $400\,\mathrm{MW_e}$; Alqahtani and Patiño-Echeverri [3] use, in their study, $50\,\mathrm{MW_{th}}$ into a CCGT of $500\,\mathrm{MW_e}$ and state that the contribution usually is lower than 15%, while other authors suggest 20% [4], like in [16]. Indeed, very few proposals can be found proposing higher contributions, like in Ref. [17], with a share of 27%, or in Ref. [18], which introduces $40\,\mathrm{MW_{th}}$ within $90\,\mathrm{MW_e}$.

For a larger solar contribution, CSP can be hybridised with auxiliary steam generators instead of integrated into CCGT [13]. This solution is often proposed for gas hybridisation [19, 20] and also for biomass [21, 22]. However, they lose the main advantage of the ISCC, which is the high heat-to-electricity conversion efficiency from both resources, particularly from the fuel one.

On the other hand, ISCCs are continuously working at variable conditions [23, 24], since the solar resource is continuously changing, which can introduce some issues [17, 25]. They consist of a specific definition of the control system [24] to ensure reliable operation, the selection of the best strategy for saving fuel [26] according to a given scenario, as well as to determine specific technological features like the influence of the heat transfer fluid temperature of the CSP plant [23] or the influence of the surplus of steam production on the steam turbine performance [27].

The problems introduced by the variability of the solar resource can be mitigated by introducing a thermal energy storage (TES) system. Since the solar contribution is small in ISCC, the TES systems are not usually considered. However, some works do consider a small TES as a buffer [24, 26, 27], concluding that it could be beneficial for improving its reliability. In those works, the TES is implemented through a single tank, and also in the form of a cascade thermal storage system [5] covering a wider temperature range. Despite that the TES would be useful and even feasible, the small solar contribution is still present.

Several works have introduced an interesting solution that uses TES systems to increase the solar contribution in ISCC-like or combined cycle plants. It consists of the integration of a conventional TES, i.e., a dual molten salt tank system, which is fed not only by the solar field but also by the exhaust gases coming from the gas turbine, that decouples the gas turbine from the steam cycle operation. This alternative has been proposed twice in different concepts. The project HYSOL [28] analysed the solution for the case of a large central tower receiver and a large gas turbine feeding the TES. Besides, the project SDCC [29] proposed the concept for multitower solar fields with multiple solarised minigas turbines, one in each tower and all of them feeding a large TES. Both solutions enable a high solar contribution, but, due to the limitations for the temperature of the cold tank of the TES, the exhaust gas temperature of the gas turbines after heating the TES is still high, preventing the system from a good heat recovery and, therefore, a good thermal efficiency.

The present work contributes to overcoming the two mentioned main drawbacks of ISCCs while maintaining the synergies. Particularly, the aim is to maximise the nominal solar contribution—around $100\,\mathrm{MW_e}$ solar and a gas turbine of $100\,\mathrm{MW_e}$—and, similarly to the previously commented solutions, to decouple the CSP from the gas turbine with a TES to avoid variable operation along the day. To increase the efficiency and overcome the limitation of the high exhaust gas temperature, two energy management systems are introduced. First, some modifications are implemented at the feedwater line of the steam cycle to simultaneously reduce the steam bleeding from the turbine and increase the heat recovery from the exhaust gases, namely, the low-temperature energy management system. Also, a recuperator is included to maximise the fuel saving in days with good solar irradiation (similar to the partial recuperation presented in Ref. [30]), which is called a high-temperature energy management system.

Section 2 shows the CCGT and CSP configurations that are considered as the reference. Section 3 firstly shows a hybrid configuration including the low-temperature energy management system and discusses the improvement and drawbacks that introduces. Afterwards, it presents an enhanced hybrid configuration that also includes the high-temperature energy management system. Section 4 presents the methodology for the analysis and the selected strategies for power generation. Section 5 is dedicated to the results. Finally, the conclusions are presented.

2. Reference Configurations

2.1. Reference CSP Plant. Figure 1 shows the layout of the plant that is considered as the reference standalone CSP configuration for comparative purposes. It consists of two heliostat fields with a central tower receiver (CTR) each, a dual tank TES system, a molten salt steam generator (MSSG), and a steam cycle (SC).

The main features of the power plant are presented in Table 1. The nominal power rate of the power plant is $100\,\mathrm{MW_e}$. The TES system is sized to supply energy during $12\,\mathrm{h}$, and the solar multiple is 2.4. Accordingly, each receiver provides $300\,\mathrm{MW_{th}}$ at nominal conditions. All these features are common in the state-of-the-art of CTR plants [31].

The layout of the MSSG is shown in Figure 2.

2.2. Reference CCGT Plant. To draw comparisons, a standard CCGT power plant was also defined. This configuration sends the exhaust gas from the gas turbine (GT) to a dual pressure-level heat recovery steam generator (HRSG) that feeds the Rankine cycle's steam turbine. Figure 3 depicts its layout, while Table 2 shows its design parameters and performance at nominal conditions.

The layout of the HRSG is the same as that of the MSSG, depicted in Figure 2, but working with gas instead of molten salts.

3. Basic and Enhanced Hybrid CSP-CCGT

As it was previously commented, the objective of the work is to significantly increase the solar contribution over the current state-of-the-art ISCC plants maintaining synergies, shipping from roughly 20% of nominal solar thermal power over the power rate of the plant to a configuration able to
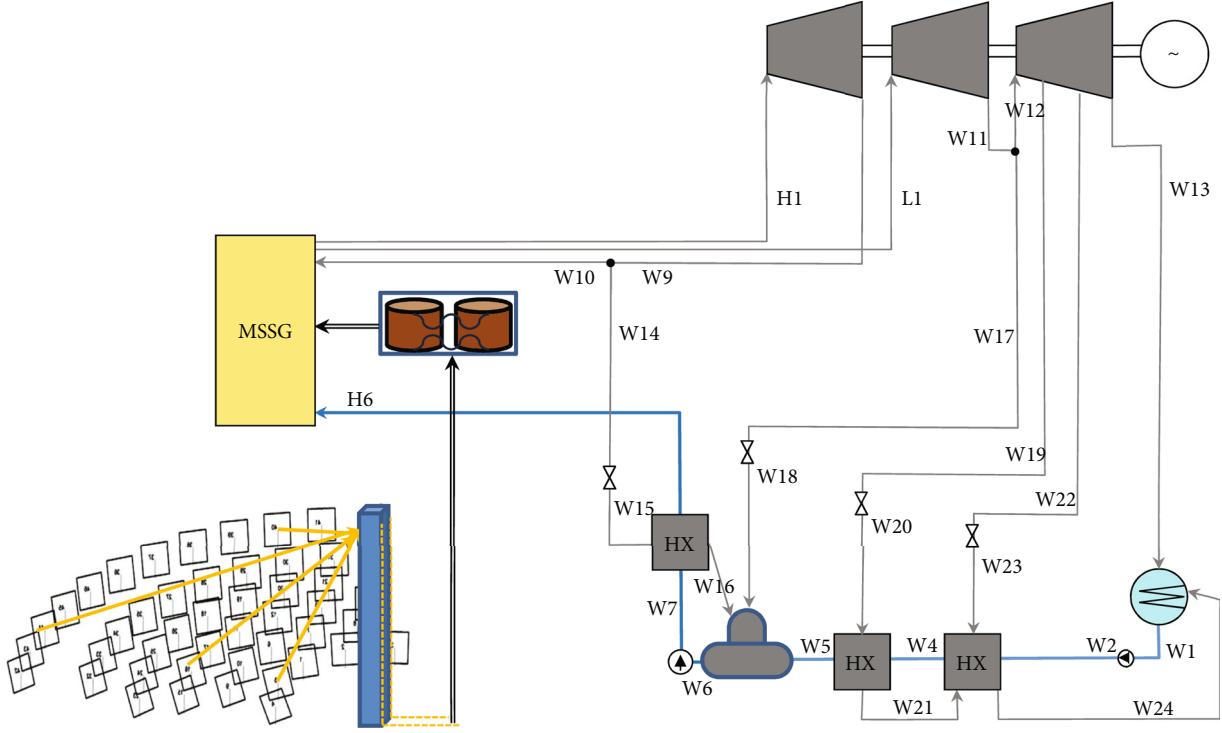
Figure 1: Layout of the reference CSP configuration.

Table 1: Main features of the reference CSP configuration.

Power rate	100 MW$_e$	T_{reheat}	470°C
Thermal efficiency	41.4%	p_{reheat}	90 bar
Solar multiple	2.4	$\eta_{s,steam\ turbine}$	90%
CTR power	600 MW$_{th}$	$\eta_{s,pumps}$	75%
TES size	12 h	$p_{condenser}$	56 mbar
$T_{hot\ tank}$	560°C	$p_{deaerator}$	3.5 bar
$T_{cold\ tank}$	280°C	TTD at preheaters	3 °C
T_{steam}	550°C	PP at MSSG	10°C
p_{steam}	160 bar	AP to drums	30°C
$T_{feedwater}$	220°C	$\eta_{electro-mechanic}$	98%

provide 100 MW$_e$ nominal from the solar resource and also using a GT of 100 MW$_e$.

The purpose of the proposed configuration is to improve the performance of the plant in terms of duty and costs over those obtained by the reference plants, CCGT and CSP, working independently.

3.1. Basic Hybrid CSP-CCGT Plant. The first key element for the proposed hybridization is the integration of a dual tank TES system that enables the decoupling of the GT from the SC. Additionally, in order to maximise the heat recovery from the exhaust gases of the GT, a low-temperature energy management system is included.

Figure 4 shows the layout of the configuration. One can observe that the configuration consists of a GT similar to the reference CCGT's one, a SC similar to the reference CSP's one, and a conventional TES system. The exhaust gases of the GT are directed to the HRSG where they generate steam in parallel to the MSSG of the CSP part of the plant. But, unlike in conventional CCGTs, the low-temperature part of the HRSG is used to heat up not only the fraction of water that is used in the HRSG but also part of the feedwater that goes to the MSSG (water stream of point W8′ in Figure 4). This additional contribution of the exhaust gases is sized to maximise the heat recovery, keeping the stack temperature at 90°C to avoid acid condensation. Besides, as part of the feedwater of the CSP plant is heated in the HRSG, the requirement of steam from the turbine bleedings decreases, increasing the power rate of the steam turbine.

The new design of the HRSG is detailed in Figure 5.

Table 3 shows the main changed parameters of the hybrid CSP-CCGT plant over the reference ones. In order to fairly compare the different configurations and, thus, quantify the synergies generated by the hybridization, the GT is the same as in the reference CCGT plant, and the capacity ($\dot{m}_{in} \cdot \sqrt{T_{in}/p_{in}}$) of the steam turbine is the same as in the reference CSP plant, as well as the solar field and the size of the TES.

Beyond the improvement that one can expect from the optimized heat recovery in the HRSG and the higher power rate in the steam turbine—due to lower steam mass flow through the turbine bleedings—another advantage of the hybridization is that there is no need for a specific steam turbine for the CCGT, as it used the turbine of the CSP plant instead.
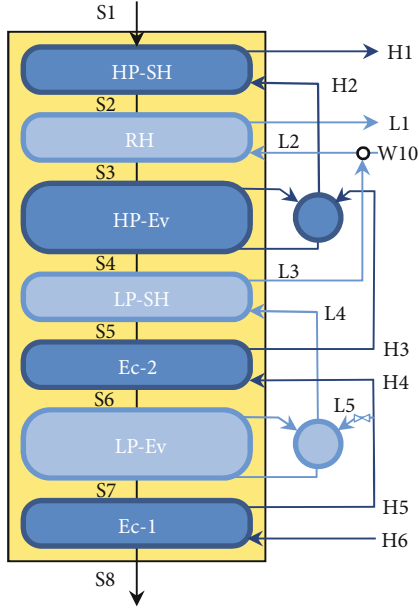
FIGURE 2: Layout of the MSSG.

However, there is an important drawback to this configuration, which is a high dumping solar energy. Specifically, as part of the steam is generated in the HRSG, the requirement of thermal power from the TES is lower. Thus, in days with high solar irradiation, there is the possibility of having the TES completely charged soon, with no possibility of discharging it afterwards. To mitigate this effect, an increased TES of 16 h is analysed in addition to the reference case of 12 h.

3.2. Enhanced Hybrid CSP-CCGT Plant. To solve the above drawback, an enhanced layout is proposed, which is shown in Figure 6. The proposed solution includes a modification at the GT and the high-temperature side of the HRSG. As in Ref. [30], the GT includes a recuperator to preheat the air coming from the compressor before it enters the combustion chamber. On days with low solar contribution, this recuperator is not used, and the system works as in the previous basic configuration. However, on days with high solar contribution, the gas at the outlet of the GT is directed to the recuperator. There, it transfers part of its residual thermal energy to the air, to save fuel in the combustion chamber. After that, it is sent to the intermediate part of the HRSG, where it is still able to produce a fraction of the high-pressure steam at saturated conditions, which is directed to the MSSG to be superheated and later reheated. In such a way, a fuel-saving operation mode is defined.

Indeed, this mode of operation allows fuel saving in the GT without reducing its power rate, as the turbine inlet temperature and the mass flow rate are maintained. Besides, the MSSG should increase its contribution, since it must complete the steam generation at the high-pressure level and also superheat and reheat the total steam generated. Thus, the requirement from the TES is higher, and the possibility of dumping decreases.

Table 4 shows the main parameters of the enhanced hybrid CSP-CCGT configuration that change over the reference configurations, while Figure 7 details the layout of the HRSG.

4. Methodology

The simulation of the configurations at the design point is based on the mass and heat balances at steady conditions. For that, some design and technological parameters are required to define the system (shown in Tables 1–4).

The following subsections detail the models used for the off-design operation of the different equipment. The codes were developed in MATLAB. Refprop software is used for obtaining the thermophysical properties of the water steam [32], the Janaf tables were used for the air and gases of the gas turbine [33], and the properties of the Hitec molten salt were taken from Ref. [34]. The dataset with the result of the simulations of all the configurations is available in Ref. [35].

4.1. Simulation Models for the CSP Plant. The design of the two solar fields is the same. It consists of 5390 heliostats that direct the solar irradiation onto an external CTR. The simulation of the optical performance is described in Refs. [36, 37]. The simulation of the receiver is based on the methodology proposed and validated in Ref. [38].

The simulation of the TES system consists in applying the mass and energy balances to each tank considering the dynamics within each one:

$$\frac{dM}{dt} = \sum \dot{m}_{\text{in}} - \sum \dot{m}_{\text{out}},$$
$$\frac{dE}{dt} = -\dot{Q}_{\text{losses}} + \sum \dot{m}_{\text{in}} \cdot h_{\text{in}} - \sum \dot{m}_{\text{out}} \cdot h_{\text{out}}. \quad (1)$$

$\dot{Q}_{\text{losses}}$ are the thermal losses of each tank, which are calculated like in Ref. [39].

The behaviour at part load operation of the steam turbine is characterized by the Stodola-Frügel law, which relates the mass flow rate in each cylinder with the inlet pressure and temperature and the outlet pressure:

$$\dot{m} \cdot \sqrt{\frac{T_{\text{in}}}{p_{\text{in}}^2 - p_{\text{out}}^2}} = K. \quad (2)$$

For the evaluation of the isentropic efficiency, the methodology proposed in Ref. [40] is used:

$$\eta_s = \eta_{s,\text{des}} - \frac{1}{3} \cdot \left(1 - \frac{\sqrt{T_{\text{in}}}/p_{\text{in}}}{\sqrt{T_{\text{in,des}}}/p_{\text{in,des}}} \right). \quad (3)$$

Specifically, this correlation proposes a linear decrease for the isentropic efficiency of the steam turbine in the range of steam capacities ($\sqrt{T_{\text{in}}}/p_{\text{in}}$) from 100% (full load) down to 70%, with a total decrease of 10 percentual points over the nominal efficiency for such a complete range.
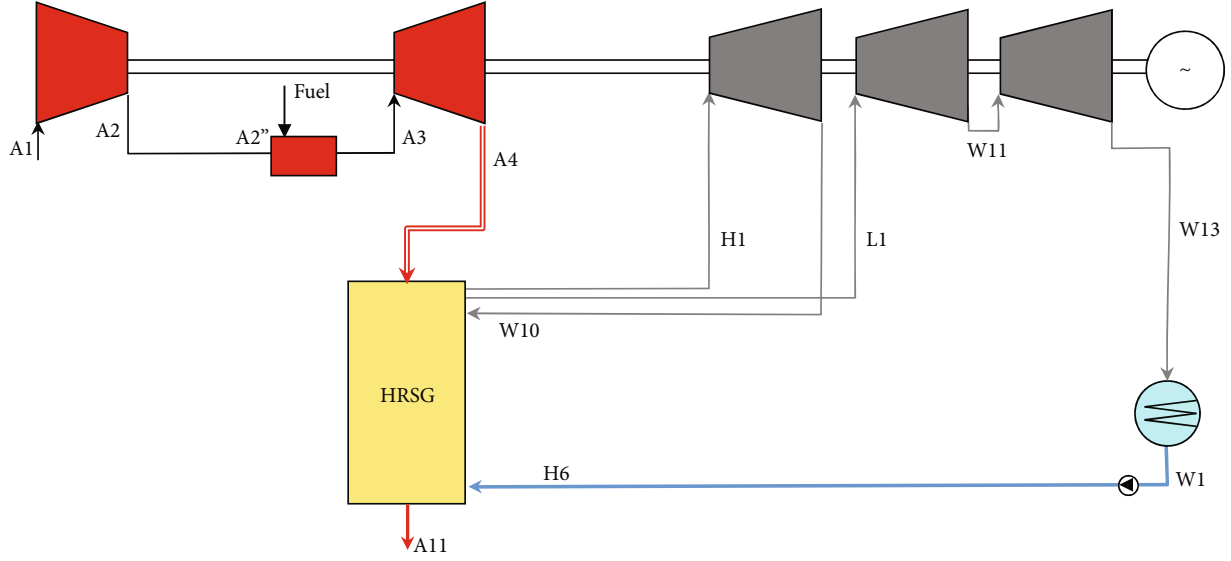
FIGURE 3: Layout of the reference CCGT configuration.

TABLE 2: Main features of the reference CCGT configuration.

GT power rate	100 MW$_e$	T_{reheat}	470°C
GT thermal efficiency	40.2%	p_{LP}	5 bar
Compression ratio	20 : 1	$p_{condenser}$	56 mbar
Turbine inlet temperature	1300°C	$\eta_{s,compressor}$	90%
$T_{stack\ HRSG}$	101.7°C	$\eta_{s,GT}$	90%
SC power rate	44.1 MW	$\eta_{s,steam\ turbine}$	90%
CCGT efficiency	57.9%	$\eta_{s,pumps}$	75%
$T_{exhaust\ gas}$	596°C	PP at HRSG	10°C
T_{steam}	550°C	AP to drums	30°C
p_{HP}	160 bar	$\eta_{electro-mechanic}$	98%

The condensation pressure of the Rankine cycle is set assuming that the saturation temperature is 10°C higher than the ambient temperature.

Finally, the off-design performance of the heat exchangers is simulated considering the following variation of the overall heat transfer coefficient:

$$\frac{U}{U_{des}} = \left(\frac{\dot{m}}{\dot{m}_{des}}\right)^n, \tag{4}$$

where $\dot{m}$ is the mass flow rate of the molten salt in the case of the MSSG and feedwater in the case of the preheaters and n takes the value of 0.8 since the Prandtl number of the flows is about 5-7.

4.2. Simulation Models for the CCGT Plant. The compressor of the GT takes air from the ambient. The compressed air goes directly to the combustion chamber (reference CCGT and basic hybrid CSP-CCGT) or via the recuperative heat exchanger (enhanced hybrid CSP-CCGT). The working pressure is fixed by the compressor pressure ratio. A pressure drop of 20 mbar is considered at the compressor inlet. The compression is simulated as a nonreversible and adiabatic process, so an isentropic efficiency is taken into account. The compressed air is then mixed with natural gas and enters the combustion chamber considering a pressure drop of 5%. After the combustion, the resulting gas flows into the turbine, where it undergoes an adiabatic and nonreversible expansion process. The pressure at the turbine outlet is known, as it is equal to the ambient pressure plus a slight pressure drop at the HRSG of 40 mbar. To account for the irreversibility of the process, an isentropic efficiency is also considered.

The variation of the isentropic efficiency of the compressor and the turbine as well as the relation between the pressure ratio and the mass flow rates at these components are estimated using the characteristic curves from Refs. [41, 42].

When the enhanced hybrid CSP-CCGT configuration operates in the fuel-saving mode (i.e., the days with high solar irradiation), in addition to the heat balance at the recuperator, an estimation for its pressure drop at the air side is required [43]:

$$\xi_{R,gt} = \frac{(\varepsilon - 0.48)}{30}, \tag{5}$$

where ξ is the pressure drop at the recuperator, which depends on the total heat exchange surface that, in turn and for this kind of heat exchangers [43], can be calculated through its effectiveness at the design conditions (ε). This effectiveness is defined as the actual temperature increase at the air side (stream with lowest heat capacity in the heat exchanger) and the maximum available temperature increase (for infinite heat exchange area):

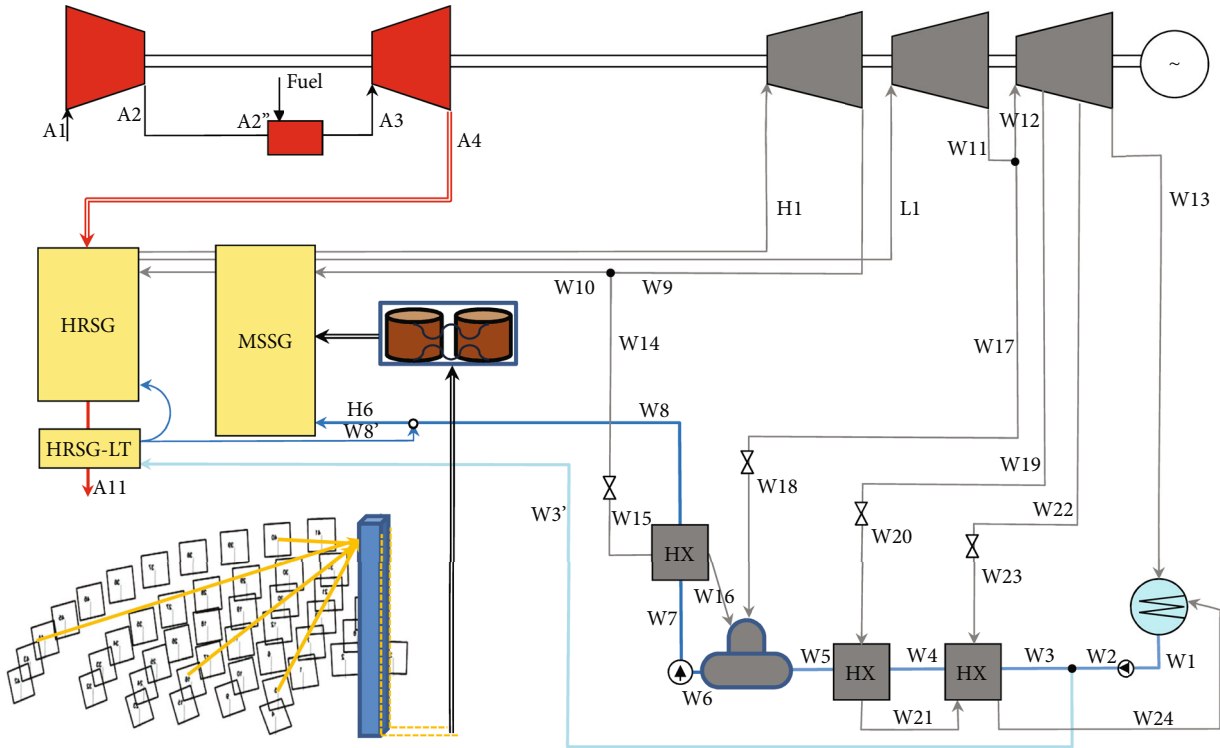$$\varepsilon = \frac{T_{A2''} - T_{A2}}{T_{A4''} - T_{A2}}. \tag{6}$$
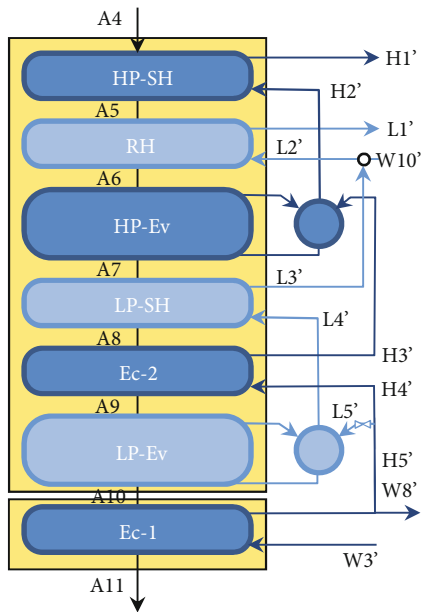
FIGURE 4: Basic hybrid CSP-CCGT plant.

FIGURE 5: Layout of the HRSG for the basic hybrid CSP-CCGT configuration.

TABLE 3: Main changed features of the basic hybrid CSP-CCGT over the references.

SC power rate	117.8 MW
SC efficiency	44.1%
TES size	12 h (reference) or 16 h (extended)

At part load operation, all the heat exchangers that are fed by the exhaust gases (i.e., those of the HRSGs as well as the recuperator) are simulated using Equation (4) but considering an exponent of 0.625, since the Prandtl number of the gas is about 0.7.

4.3. Site for the Plant and Scenarios of Production. The plant is assumed to be placed in Seville (Spain). For the site, the weather and the solar irradiation data are available in an hourly basis [44].

The reference CSP plant has a solar multiple of 2.4 and includes a TES system to drive the power block at full load during 12 h. These features enable the plant to work up to 24 h on summer days with good solar irradiation. When the solar resource is not so high, the periods of the day with the highest electricity demand (according to the usual electricity market in Spain) are selected as a priority. These peak periods take place early in the morning and early in the evening. Once such periods are covered, the interim time between them and the two last hours of the day are selected. The night period between the midnight and the first peak of the next day is finally completed. The priority is shown in Table 5.

There are two possibilities for the reference CCGT to operate. The first choice is the operation in baseload, working 24 h a day. The other choice is the operation as a peak plant during the highest demand periods. With the objective of showing the synergies and seeking for the clarity, the baseload scenario is selected.

The proposed basic hybrid CSP-CCGT plant works similarly to the reference ones. The CSP part of the plant
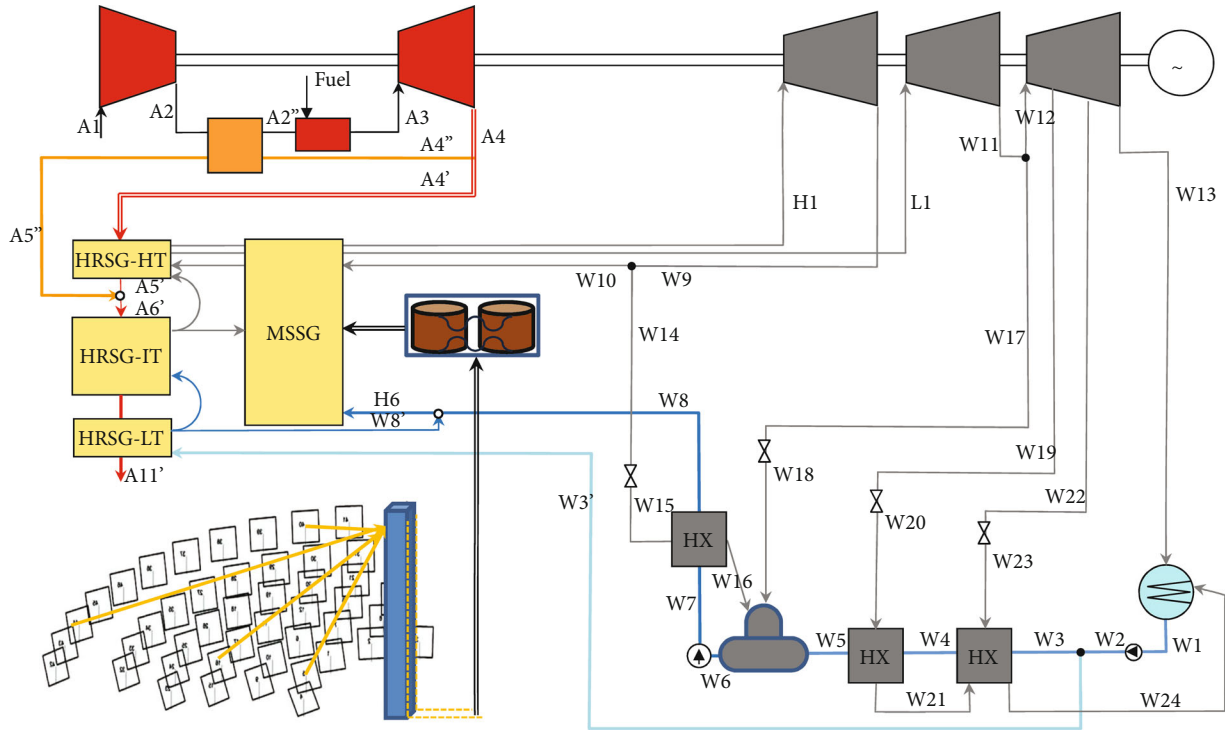
FIGURE 6: Enhanced hybrid CSP-CCGT plant.

TABLE 4: Main changed features of the enhanced hybrid CSP-CCGT over the references.

Nominal thermal power at the recuperator	61 MW$_{th}$
TTD at the recuperator	10°C
$T_{stack\ HRSG}$	90°C
ST power rate	123.6 MW
η_{SC}	46.1%
TES size	12 h (reference) or 16 h (extended)

prioritizes the working time according to Table 5, while the CCGT part works at the baseload scenario.

Finally, the selection of the schedule for operation of the enhanced hybrid CSP-CCGT plant requires a previous step, which is to decide whether or not to operate the GT at the fuel-saving mode. In this regard, two strategies are selected, maximising either the energy generation—namely, boosting strategy—or the fuel saving—saving strategy.

For the boosting strategy, the fuel-saving mode of the gas turbine is only active on days when the expected solar contribution plus the expected heat recovery from the exhaust gases exceeds the total requirement for the CSP part of the plant to operate 24 h. The number of hours working at this mode is estimated to avoid solar dumping. The time selected to start the fuel-saving mode is the same as the CTR start working, and it is maintained provided that the MSSG is operative and that there is enough energy in the TES.
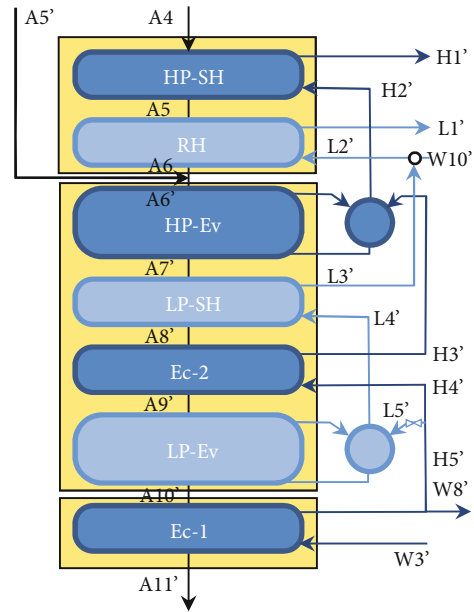

FIGURE 7: Layout of the HRSG for the enhanced hybrid CSP-CCGT configuration.

For the saving strategy, the fuel-saving mode is always active provided that the CSP part of the plant is operative. If the CSP part plant is shut down, the GT works at the regular mode (without the recuperator) because, otherwise, it is not possible to generate superheated and reheated steam.

TABLE 5: Priority for operation.

	1st	2nd	3rd	4th	5th	6th	7th	8th	9th	10th	11th	12th	13th	14th	15th	16th	17th	18th	19th	20th	21st	22nd	23rd	24th
Priority (h)	20	21	22	9	8	7	19	10	23	11	18	24	12	13	14	17	15	16	1	2	3	4	5	6

4.4. Figures of Merit

4.4.1. Thermal Performance.
The yearly production is the sum of the energy generated each hour of the year. For the reference CSP plant, the average thermal efficiency of the power block is the total yearly energy divided by the solar energy collected by the CTR once it discounted the optic and thermal losses of the solar field and the receiver:

$$\eta_{\text{CSP}} = \frac{E_{y,\text{CSP}}}{Q_{\text{sol},y,\text{CSP}}}. \tag{7}$$

Likewise, for the reference CCGT, the average thermal efficiency of the plant is the ratio of the yearly energy production to the thermal power supplied by the fuel:

$$\eta_{\text{CCGT}} = \frac{E_{y,\text{CCGT}}}{Q_{y,\text{fuel}}}. \tag{8}$$

The energy supplied by the fuel ($Q_{y,\text{fuel}}$) is the sum along the year of the product of fuel mass flow rate times the lower heating value of the fuel (48 MJ/kg for natural gas), which is calculated hourly.

To jointly assess the performance of the reference CSP and CCGT plants working separately, an overall heat rate is defined, which provides a magnitude to quantify the use of fossil resource over the total electricity production:

$$\text{HR} = \frac{Q_{y,\text{fuel}}}{E_{y,\text{CSP}} + E_{y,\text{CCGT}}}. \tag{9}$$

Equation (9) can be also used when assessing the performance of the hybrid configurations. However, to compare the behaviour of the CSP and CCGT parts of the hybrid configurations with the behaviour of the reference CSP and CCGT plants, respectively, it is necessary to quantify the solar and fuel contribution over the total yield, particularly in the SC, since the GT is totally driven by the fuel. For that, the same methodology as in Refs. [30, 45] is followed. Specifically, this methodology sets the weights of each source as proportional to the exergy content of the heat transferred from the energy source to the working fluid of the power cycle, i.e., from either the molten salt or the exhaust gases to the steam/water of the SC, which is also evaluated hourly:

$$\dot{W}_{\text{sol}} = \dot{W}_{\text{SC}} \cdot \frac{\dot{Ex}_{\text{MS}\longrightarrow\text{water}}}{\dot{Ex}_{\text{MS}\longrightarrow\text{water}} + \dot{Ex}_{\text{gas}\longrightarrow\text{water}}},$$

$$\dot{W}_{\text{fuel}} = \dot{W}_{\text{SC}} \cdot \frac{\dot{Ex}_{\text{gas}\longrightarrow\text{water}}}{\dot{Ex}_{\text{MS}\longrightarrow\text{water}} + \dot{Ex}_{\text{gas}\longrightarrow\text{water}}}. \tag{10}$$

TABLE 6: Economic scenario [46].

Surcharge for construction, engineering, and contingencies	10%
CCGT O&M cost	17.9 €/(year·kW)
CSP O&M cost	2.4 c$/kWh
Interest rate	4%
Life	25 years
O&M escalation rate	1%
Fuel escalation rate	2.5%
Price of natural gas	4 c€/kWh

TABLE 7: Models for cost allocation.

Specific cost of the CCGT plant [47, 48]	$(466,1 + 113900/P[\text{MW}])$ €/kW
Specific cost of the CSP plant [49]	7890 €/kW
Specific cost of the SC of the CCGT [50]	860 $/kW
Cost of the recuperator [51]	$(2861 \cdot A^{0,59}[\text{m}^2])$ $
Specific cost for the TES [52]	19.75 $/kWh

Once the power contribution on the SC has been allocated ($\dot{W}_{\text{sol}}$ and $\dot{W}_{\text{fuel}}$), the yearly contributions ($E_{y,SC-\text{sol}}$ and $E_{y,SC-\text{fuel}}$, respectively) are the sum of the hourly energy contribution over the year. Finally, the average yearly efficiencies are

$$\eta_{\text{CSP}-\text{part}} = \frac{E_{y,\text{SC,sol}}}{Q_{\text{sol},y,\text{CSP}}},$$

$$\eta_{\text{CCGT}} = \frac{E_{y,\text{GT}} + E_{y,\text{SC}-\text{fuel}}}{Q_{y,\text{fuel}}}. \tag{11}$$

4.5. Economic Analyses.
From an economic perspective, the best parameter to compare the different configurations is the levelized cost of energy (LCOE), which is the ratio of the levelized costs of investment (LC_{inv}), plus the levelized cost of operation and maintenance (LC_{OM}), plus the levelized cost of fuel (LC_f) to the yearly energy production:

$$\text{LCOE} = \frac{\text{LC}_{\text{inv}} + \text{LC}_{O\&M} + \text{LC}_{fuel}}{E_{y,\text{total}}}. \tag{12}$$

These levelized costs require the definition of an economic scenario, which is shown in Table 6.

To compare the results of the reference configurations working separately with those of the hybrid plants, a joint
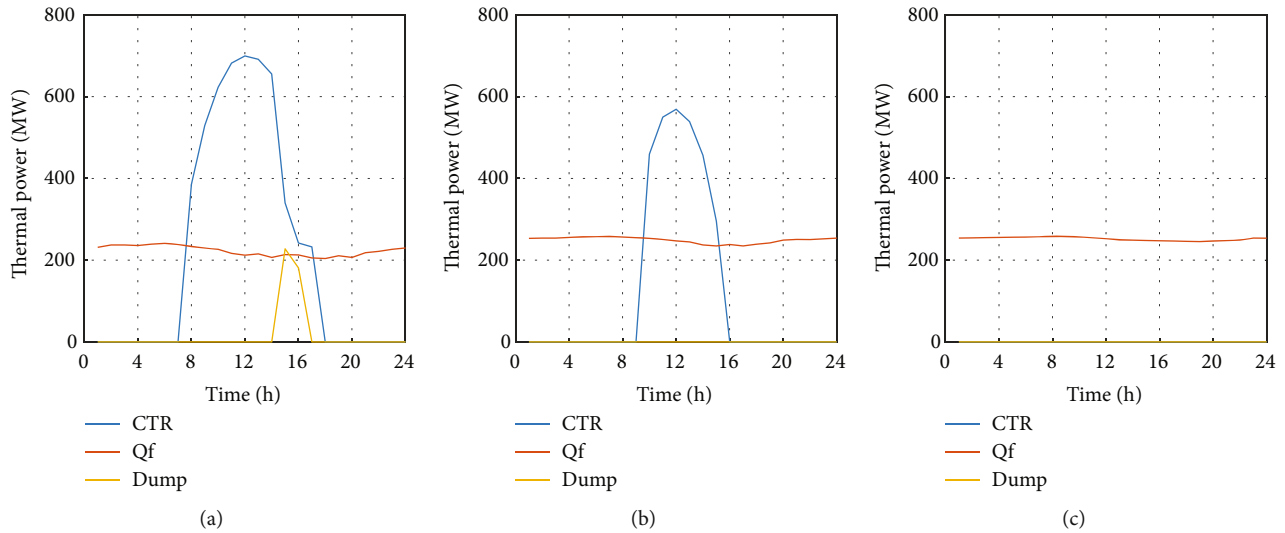
FIGURE 8: Fuel and solar resources used by the reference configurations in the good (a), intermediate (b), and bad (c) days.

LCOE for the reference plants is calculated considering the sum of the levelized costs of both plants in the numerator of Equation (12) and the sum of the yearly production in the denominator.

Table 7 presents the data used to calculate the capital expenses of the reference CSP and CCGT plants. The basic hybrid CSP-CCGT configuration removes the steam turbine of the power block and, as it was commented in Section 3.1, considers an additional case with an extended TES. The enhanced hybrid CSP-CCGT plant also removes the steam turbine of the CCGT but includes the recuperator of the GT. The additional case with an extended TES is also considered. The costs related to these modifications must be accordingly either subtracted (if the equipment is removed) or added (if it is included). The costing models for them are also shown in Table 7.

5. Results

5.1. Operation of the Reference and Proposed Configurations

5.1.1. Reference CSP and CCGT Plants. Figure 8 shows the fuel resource used for the reference CCGT plant as well as the useful solar energy at the CTRs and the dumped solar energy. To show the behaviour, three different days are selected with good, intermediate, and bad solar irradiation (July-21st, Nov-12th, and Jan-26th, respectively).

One can observe that the fuel consumption is fairly constant within the day and throughout the year, provided that the reference CCGT is working at full load 24 h a day. Besides, during the good day, the energy collected by the CSP plant is enough for charging the TES, and even it is required some solar dumping. In the intermediate day, the solar resource is quite lower, and there is no need for dumping. Finally, in the bad day, there is no solar resource.

Figure 9 shows the performance of the reference CSP and CCGT plants. Regarding the CCGT, it is observed that the power rate of the GT is lower during the central part

of the day due to the higher ambient temperature. The behaviour of the CCGT is the same, as its performance is dominated by the GT.

Regarding the CSP plant, it is observed that, in the good day, the power plant is working all day except from 5:00 to 7:00, because the day before the solar resource was not enough to keep the plant working 24 h. Besides, there was not enough stored energy to allow the operation of the plant during the complete morning peak, as it is later explained. In the intermediate day, it is decided to prioritize the plant operation at the evening rather than at midday. Finally, in the bad day, the plant is switch off the whole day except for the morning peak, thanks to the energy stored during the previous day, which prioritized the operation during this morning peak over the previous midday.

The information above is completed with Figure 10, which shows the state of the hot tank of the TES these three days. At the beginning of the good day, theoretically, there was energy available to work until 4:00 and then to start operating again at 7:00. Such forecast is done for the day prior to perform the simulations (with a grid-step of 1 h) and assuming nominal temperature change for the molten salts in the SSG. However, the forecast can fail after the simulations of the day are done because the temperature of the cold tank continuously varies, with a slight effect on the energy that can be supplied. Thus, the actual energy at the TES for the good day after 4:00 was 0.96 h instead of higher than 1 h, so the start-up at 7:00 was not finally possible (with the mentioned time step of 1 h). At the end of the day, again, there are 5 h available at the TES to operate during the night and in the next morning peak. In the intermediate day, the energy available at the beginning of the day is used from 7:00 to 9:00. Then, the TES is charged, and, as there is not enough solar resource to operate the whole day, the discharge starts at 17:00, leaving 3 h available for the next morning peak. Finally, the operation in the bad day is only possible at the morning peak thanks to the energy stored during the day before. However, the TES is
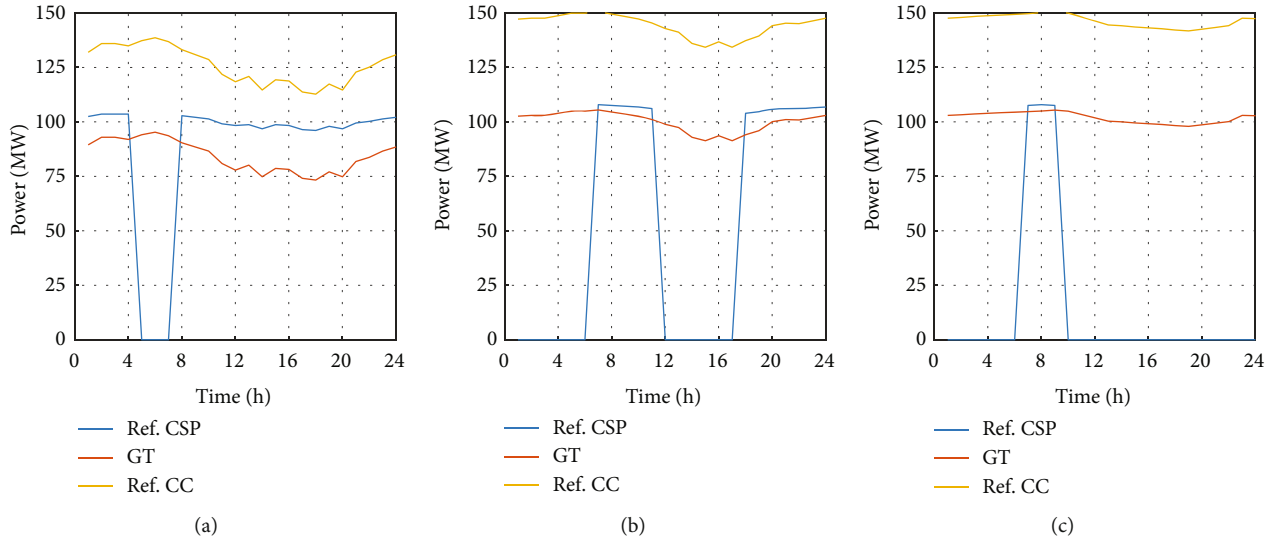
FIGURE 9: Power generated power by the reference configurations in the good (a), intermediate (b), and bad (c) days.
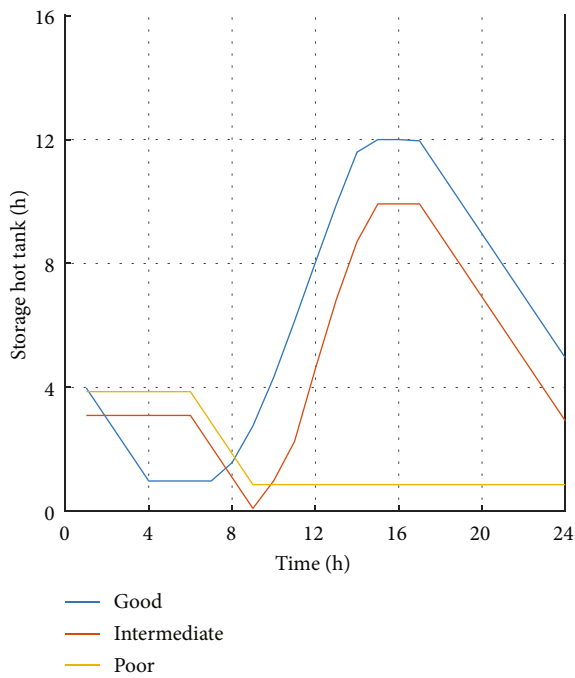

FIGURE 10: TES state of the reference CSP plant in the good, intermediate, and bad days.
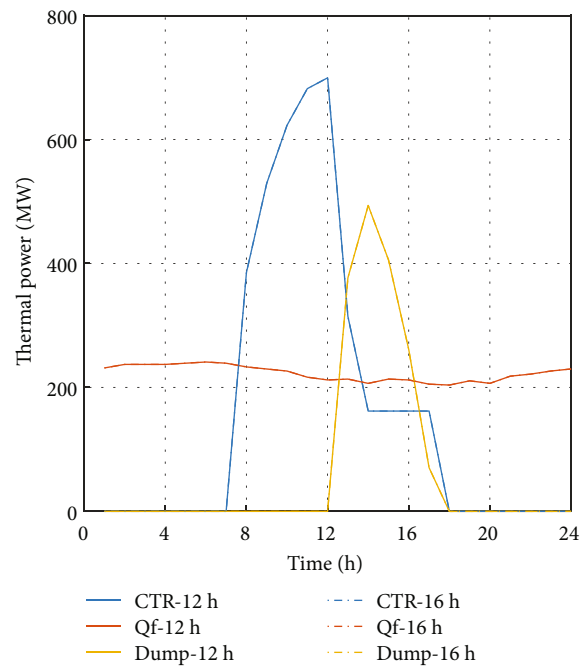

FIGURE 11: Fuel and solar resources used by the basic hybrid CSP-CCGT configuration in the good day.

discharged since 9:00 due to the absence of solar resource. Thus, there is no energy available for the morning of the next day.

5.1.2. Basic Hybrid CSP-CCGT Plant. In this case, the solar and fuel resources are the same as for the reference configurations, because the systems are the same. The only difference, depicted in Figure 11, is that, on the good day, the dumping energy is higher than in the reference CSP plant. This is because the energy required by the MSSG is lower than in the reference configuration. The figure is presented for the two considered TES, the regular of 12 h and the extended of 16 h, both reaching the same dumping, as it is later explained.

The performance of the GT and the SC are presented in Figure 12. The GT behaves the same as in the reference case. The CSP part, due to the lower heat requirement of the MSSG, is able to operate 24 h. The low heat requirement in the MSSG is particularly noticed on days with intermediate solar resource. This day, the basic hybrid configuration can operate not only at the peaks but also from 12:00 to
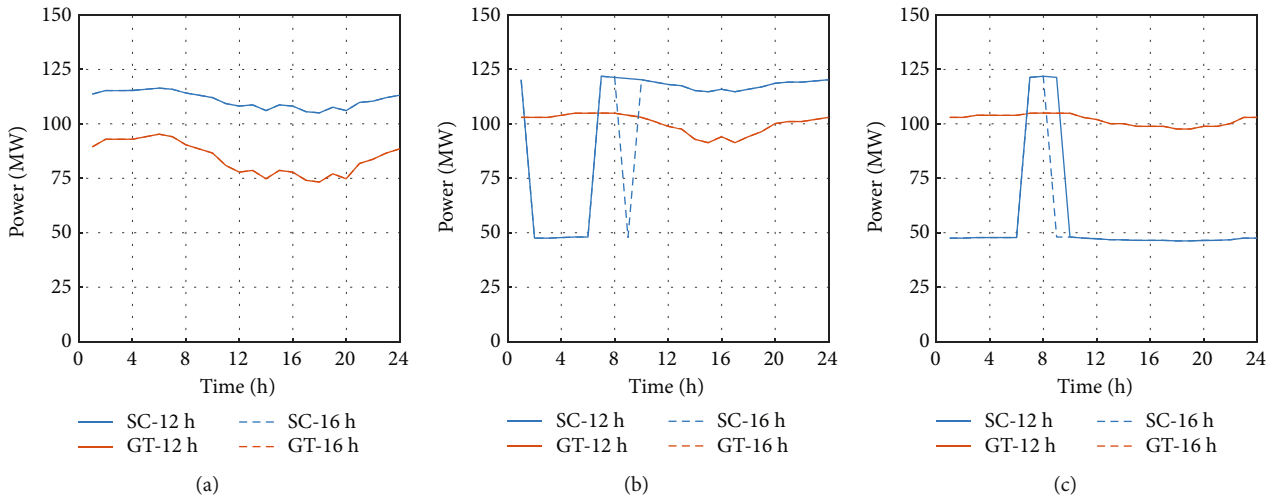
FIGURE 12: Power generated power by the steam cycle and the gas turbine of the basic hybrid CSP-CCGT plant in the good (a), intermediate (b), and bad (c) days.
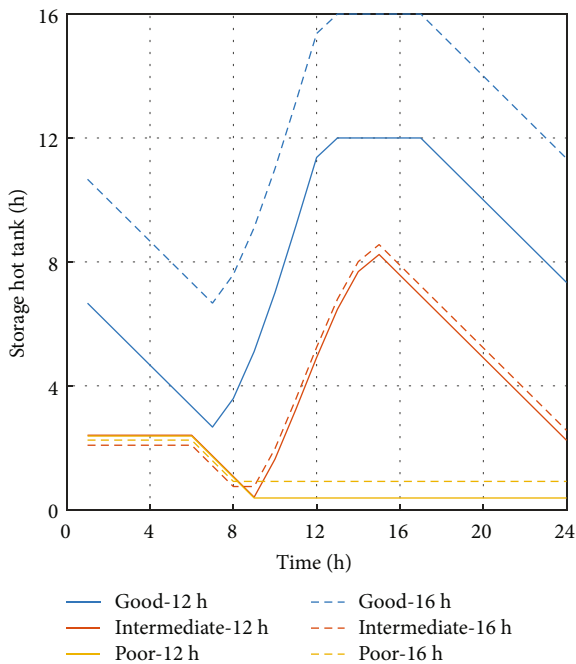

FIGURE 13: TES state of the basic hybrid CSP-CCGT plant in the good, intermediate, and bad days.

17:00. Finally, there are no significant differences in the bad day due to the null solar resource.

Figure 13 shows the TES state for the basic hybrid CSP-CCGT configuration during the three selected days. As the main result, one can observe that the slope for the discharging process is lower than those shown in Figure 10, because the required molten salt mass flow rate is lower. This low mass flow rate makes the TES be charged sooner, and, moreover, it avoids a complete discharge of the system. Such behaviour is especially prejudicial in summer, when it operates between midcharge state and full charge regardless of the size of the TES.

5.1.3. Enhanced Hybrid CSP-CCGT Plant. Figure 14 shows the fuel and solar resources used for the operation in the selected days. It can be observed that the fuel consumption during the good day is lower than for the other configurations, since the GT is working at the fuel-saving mode for a large time of the day. This happens using the boosting strategy, both considering the regular TES, and even more time considering the extended one. And it also takes place for the saving strategy, in this case, maximising the fuel-saving during the whole day. On days with intermediate solar resources, the GT does not work at this operation mode unless the saving strategy is selected. It is observed that, for the boosting strategy, the starting time for the fuel-saving mode is at 7:00. At 9:00, it stops because there is not enough molten salt stored. Later, it is again started and maintained while the CSP part of the plant is operative. Finally, it is observed that, in this configuration, the issue of excessive dumping disappears.

Figure 15 shows the generated power. In the good day, it is possible to operate during the 24 h regardless of the strategy (boosting or saving) in the case of the extended TES. In the intermediate day, the boosting strategy is able to drive the plant between the morning and evening peak, because it works at the regular mode (without the recuperator), similarly to the basic hybrid CSP-CCGT one, with low heat requirement in the MSSG. However, it is not possible when selecting the saving strategy. In the bad day, the behaviour is the same regardless of the strategy.

Figure 16 shows the TES state for the different strategies. One can observe that dumping is not an issue for this configuration and that there is no need for an extended TES of 16 h from a behavioural perspective.

5.2. Comparison of the Yearly Performance. Table 8 shows the results of the configurations over the year from a technical point of view. The energy produced by the GT and the fuel consumption are basically the same for the reference CCGT and the basic hybrid CSP-CCGT plant. The small differences are attributed to the allocation of the fuel and solar
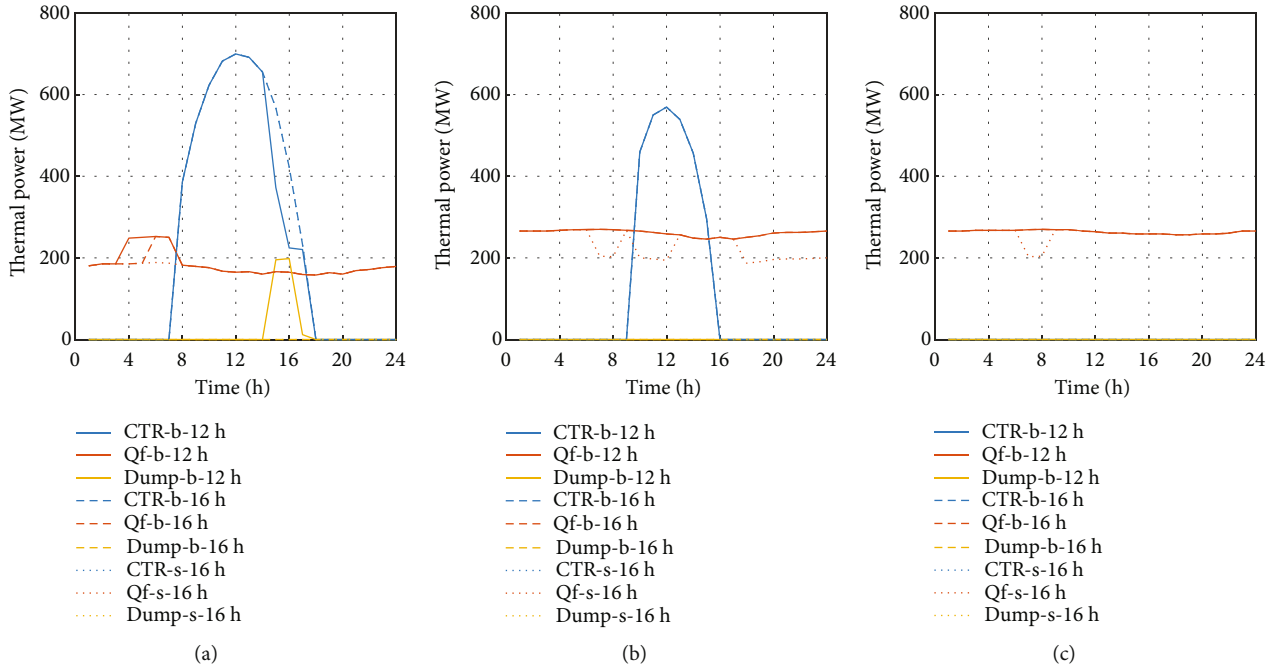
FIGURE 14: Fuel and solar resources used by the enhanced hybrid CSP-CCGT configuration in the good (a), intermediate (b), and bad (c) days.
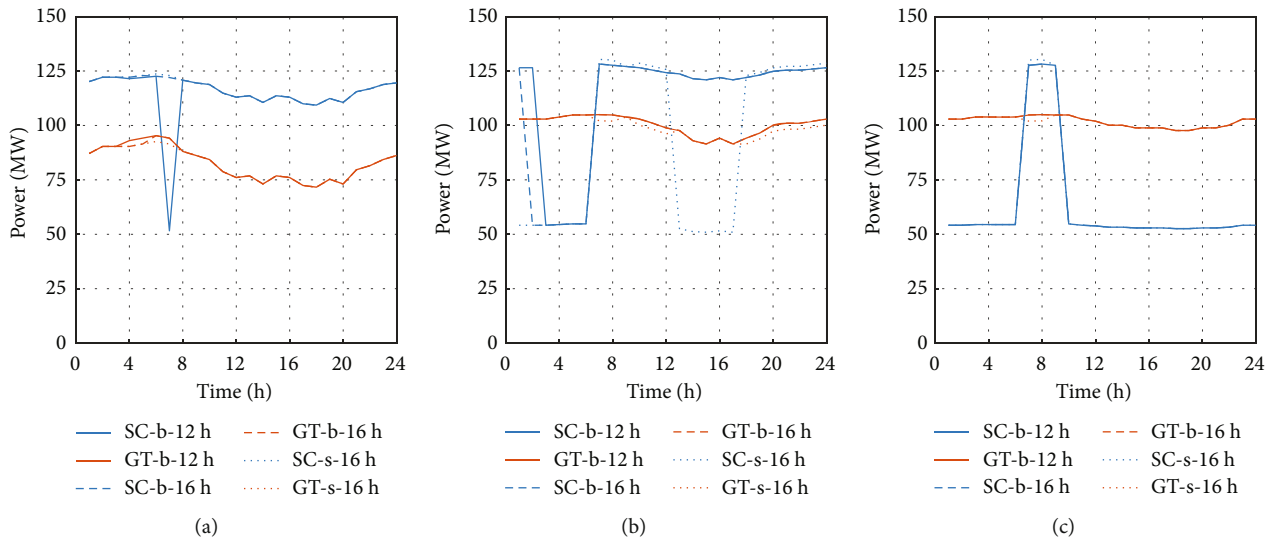

FIGURE 15: Power generated power by the steam cycle and the gas turbine of the enhanced hybrid CSP-CCGT plant in the good (a), intermediate (b), and bad (c) days.

contribution in the hybrid configuration, but they are negligible. However, the fuel consumption in the enhanced hybrid CSP-CCGT plant is lower, particularly with the saving strategy, as the recuperator is activated on the days with good solar irradiation. Likewise, the efficiency of the CCGT part is higher than in the previous configurations.

Regarding the solar contribution, the basic hybrid CSP-CCGT cannot increase the performance of the reference CSP plant due to the high solar dumping. However, the enhanced CSP-CCGT working with the boosting strategy increases the solar contribution in absolute and relative

terms. When it operates with the saving strategy, the absolute production is slightly lower, but the relative one is higher. Similarly, the configuration with the lowest heat rate is the enhanced hybrid CSP-CCGT one, while the highest value is for the basic hybrid CSP-CCGT one.

The total generated energy is quite similar in all configurations, which indicates that the hybrid configurations are able to perform the same as the reference ones working separately despite the SC of the reference CCGT is removed.

In conclusion, from a thermodynamic and technical point of view, the hybridisation is able to introduce
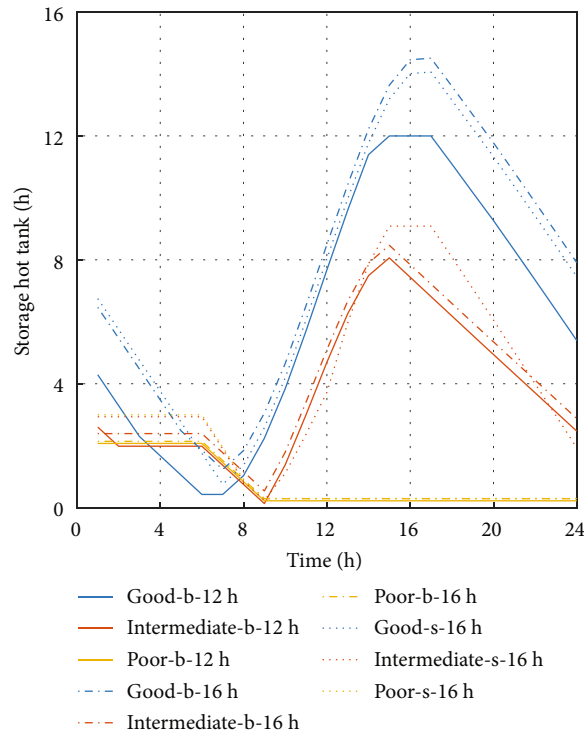
FIGURE 16: TES state of the basic hybrid CSP-CCGT plant in the good, intermediate, and bad days.

TABLE 8: Yearly performance of the configurations.

| | Reference | | | Basic hybrid CSP-CCGT | | Enhanced hybrid CSP-CCGT, boosting | | Enhanced hybrid CSP-CCGT, saving | |
	CSP	CCGT	Join	TES 12 h	TES 16 h	TES 12 h	TES 16 h	TES 12 h	TES 16 h
E_{CCGT} (GWh)	—	1221	1221	1247	1247	1244	1239	1156	1152
E_{fuel} (GWh)	—	2120	2120	2120	2120	2094	2083	1934	1926
η_{CC} (-)	—	57.6%	57.6%	58.8%	58.8%	59.4%	59.5%	59.8%	59.8%
E_{sol} (GWh)	473	—	473	421	427	478	488	457	468
E_{CTR} (GWh)	1130	—	1130	1130	1130	1130	1130	1130	1130
η_{sol} (-)	42.8%	—	42.8%	43.0%	43.0%	43.3%	43.2%	41.5%	41.5%
E_{tot} (GWh)	473	1221	1694	1668	1674	1722	1727	1613	1620
E_{dump} (GWh)	22	—	22	148	133	26	0.15	28	0.47
HR (-)		1.74	1.25	1.27	1.27	1.22	1.21	1.20	1.19
Solar contrib. (-)	—	—	27.9%	25.2%	25.5%	27.8%	28.3%	28.3%	28.9%

improvements over the reference plants working separately, but only when the two energy management systems of low- and high-temperature are considered, i.e., the enhanced hybrid CSP-CCGT configuration. The basic hybrid CSP-CCGT cannot improve the performance due to the high solar dumping, even with the extended TES of 16 h.

Finally, Table 9 shows the economic results for the different configurations and strategies of operation. First, it presents the capital expenses (CAPEX) of the reference plants, which are also applied to the proposed configurations as they have the same components. Afterwards, the costs of the components that are removed or added are consid-

ered to reach the actual CAPEX of each configuration. Finally, the levelized exploitation costs are shown, as well as the LCOE.

One can observe that the basic hybrid CSP-CCGT configuration cannot reduce the combined LCOE for the reference plants working separately. However, the enhanced hybrid CSP-CCGT configurations reach to a significant decrease in the LCOE, particularly for the boosting strategy.

In conclusion, the enhanced hybrid CSP-CCGT plant introduces higher solar contribution while improving both the thermodynamic and economic results over those obtained for the conventional plants working separately.

TABLE 9: Economic results for the different configurations.

	Reference			Basic hybrid CSP-CCGT		Enhanced hybrid CSP-CCGT, boosting		Enhanced hybrid CSP-CCGT, saving	
	CSP	CCGT	Join	TES 12 h	TES 16 h	TES 12 h	TES 16 h	TES 12 h	TES 16 h
$CAPEX_{ref}$ (M€)	789.0	181.0	1067.0	1067.0	1067.0	1067.0	1067.0	1067.0	1067.0
ΔSC_{CCGT} (M€)	—	—	—	−37.8	−37.8	−37.8	−37.8	−37.8	−37.8
ΔRec_{GT} (M€)	—	—	—	—	—	+0.6	+0.6	+0.6	+0.6
ΔTES (M€)	—	—	—	—	+12.7	—	+12.7	—	+12.7
$CAPEX_{actual}$ (M€)	789.0	181.0	1067.0	1025.4	1039.4	1026.1	1040.1	1026.1	1040.1
LC_{inv} (M€)	11.5	50.2	61.7	59.3	60.1	59.3	60.1	59.3	60.1
$LC_{O\&M}$ (M€)	3.9	17.1	19.8	19.8	19.8	19.8	19.8	19.8	19.8
LC_{fuel} (M€)	159.8	0.0	159.8	159.8	159.8	157.9	157.0	145.8	145.2
LCOE (c€/kWh)	14.35	14.22	14.24	14.32	14.32	13.76	13.72	13.94	13.89

6. Conclusions

The paper proposes two hybrid configurations, namely, basic hybrid CSP-CCGT and enhanced hybrid CSP-CCGT, with the objective of increasing the solar contribution over those reached by the state-of-the-art ISCCs, while maintaining synergies between the solar and combined cycle technologies. Both configurations are based on decoupling the gas turbine operation from the steam cycle by means of a conventional TES system.

The basic hybrid CSP-CCGT configuration introduces a low-temperature energy management system that consists of a modification at the low-temperature side of the HRSG and another one at the feedwater heating line, which allows a large heat recovery and higher power in the steam turbine. Thus, it demonstrates that it is possible to introduce synergies in a hybrid plant with a GT of 100 MW$_e$ and a CSP plant of 100 MW$_e$ while reducing the CAPEX. However, there is an issue of this configuration with the solar dumping that prevents the improvement of the yearly yield. The solar dumping makes it unable to reduce the combined LCOE over those of the reference plants working separately.

To overcome the problem of excessive dumping, the enhanced hybrid CSP-CCGT configuration introduces a high-temperature energy management system. It consists in including a recuperative heat exchanger for the GT and a modification in the high-temperature part of the HRSG. The recuperator is activated on days with high solar irradiation, so the decrease of heat recovery from the GT is balanced by a higher contribution from the CSP plant. This configuration maintains the previous synergies and CAPEX reduction avoiding the solar dumping and reaching a significant decrease in the LCOE, particularly for the boosting strategy.

As a result, the performance of the enhanced hybrid CSP-CCGT configuration is better than those reached by the reference CSP and CCGT working separately despite the steam cycle of the CCGT is removed. Indeed, it leads to higher solar generation and contribution, and to lower fuel consumption. Thanks to this behaviour and to the lower CAPEX, the LCOE decreases, being lower than those of the reference CSP and CCGT plants.

Nomenclature

Acronyms

CAPEX: Capital expenses
CCGT: Combined cycle gas turbine
CSP: Concentrating solar power
CTR: Central tower receiver
Ec: Economiser
Ev: Evaporator
GT: Gas turbine
HP: High pressure
HRSG: Heat recovery steam generator
ISCC: Integrated solar combined cycle
LP: Low pressure
MSSG: Molten salt steam generator
O&M: Operation and maintenance
RH: Reheater
SC: Steam cycle
SH: Superheater
TES: Thermal energy storage.

Symbols

AP: Approach point (K)
E: Energy (J)
$\dot{Ex}$: Exergy flow (W)
h: Specific enthalpy (J·kg^{-1}), hour
HR: Heat rate (-)
K: Steam turbine mass flow parameter $(\dot{m}_{st} \cdot \sqrt{T_i/(p_{in}^2 - p_{out}^2)})$ (m·K$^{0.5}$·s)
LC: Levelized cost (€)
LCOE: Levelized cost of electricity (€·J^{-1})
M: Mass (kg)
$\dot{m}$: Mass flow (kg·s^{-1})
p: Pressure (Pa)
PP: Pinch point (K)
Q: Thermal energy (J)
$\dot{Q}$: Thermal power (W)
t: Time (s)
T: Temperature (K)

TTD: Terminal temperature difference (K)
U: Overall heat transfer coefficient ($W\,K^{-1}\,m^{-2}$)
$\dot{W}$: Power (W).

Greek letters

Δ: Increment
ε: Recuperator effectiveness (-)
ξ: Pressure drop (-)
η_s: Isentropic efficiency
η: Efficiency (-).

Subscripts

des: Design
in: Inlet
inv: Investment
MS: Molten salt
out: Outlet
sol: Solar
tot: Total
y: Yearly.

Data Availability

The data from the simulations (MATLAB files) used to support the findings of this study have been deposited in the Zenodo repository (10.5281/zenodo.7853000).

Conflicts of Interest

The authors declare that they have no conflicts of interest.

Acknowledgments

References

[1] T. Liu, J. Yang, Z. Yang, and Y. Duan, "Techno-economic feasibility of solar power plants considering PV/CSP with electrical/thermal energy storage system," *Energy Conversion and Management*, vol. 255, article 115308, 2022.

[2] P. H. Shaikh, A. Shaikh, Z. A. Memon, A. A. Lashari, and Z. H. Leghari, "Microgrids: a review on optimal hybrid technologies, configurations, and applications," *International Journal of Energy Research*, vol. 45, no. 9, pp. 12564–12597, 2021.

[3] B. J. Alqahtani and D. Patiño-Echeverri, "Integrated solar combined cycle power plants: paving the way for thermal solar," *Applied Energy*, vol. 169, pp. 927–936, 2016.

[4] E. Okoroigwe and A. Madhlopa, "An integrated combined cycle system driven by a solar tower: a review," *Renewable and Sustainable Energy Reviews*, vol. 57, pp. 337–350, 2016.

[5] N. Khandelwal, M. Sharma, O. Singh, and A. K. Shukla, "Comparative evaluation of integrated solar combined cycle plant with cascade thermal storage system for different heat transfer fluids," *Journal of Cleaner Production*, vol. 353, article 131519, 2022.

[6] Z. W. Zhang, J. Sun, R. L. Wang, and J. J. Wei, "Comprehensive evaluation of integrated solar combined cycle system regarding fuel-savability under unified framework," *Applied Thermal Engineering*, vol. 199, article 117539, 2021.

[7] A. M. Nabati, M. S. Sadeghi, S. N. Naserabad, H. Mokhtari, and S. Izadpanah, "Thermo-economic analysis for determination of optimized connection between solar field and combined cycle power plant," *Energy*, vol. 162, pp. 1062–1076, 2018.

[8] Z. Zhang, L. Duan, Z. Wang, and Y. Ren, "General performance evaluation method of integrated solar combined cycle (ISCC) system," *Energy*, vol. 240, article 122472, 2022.

[9] A. Rovira, M. J. Montes, F. Varela, and M. Gil, "Comparison of heat transfer fluid and direct steam generation technologies for integrated solar combined cycles," *Applied Thermal Engineering*, vol. 52, no. 2, pp. 264–274, 2013.

[10] A. Rovira, C. Sánchez, M. Valdés et al., "Comparison of different technologies for integrated solar combined cycles: analysis of concentrating technology and solar integration," *Energies*, vol. 11, no. 5, p. 1064, 2018.

[11] M. T. Mabrouk, A. Kheiri, and M. Feidt, "A systematic procedure to optimize integrated solar combined cycle power plants (ISCCs)," *Applied Thermal Engineering*, vol. 136, pp. 97–107, 2018.

[12] L. H. A. E. Elmorsy, *Comparative Exergy-Based Evaluation of Standalone, Integrated and Hybrid Concentrated Solar Power Systems*, Technische Universität Berlin, Berlin, 2022.

[13] S. Pramanik and R. V. Ravikrishna, "A review of concentrated solar power hybrid technologies," *Applied Thermal Engineering*, vol. 127, pp. 602–637, 2017.

[14] A. O. Binamer, "Al-Abdaliya integrated solar combined cycle power plant: case study of Kuwait, part I," *Renewable Energy*, vol. 131, pp. 923–937, 2019.

[15] L. Duan, Z. Wang, and Y. Guo, "Off-design performance characteristics study on ISCC system with solar direct steam generation system," *Energy*, vol. 205, article 118044, 2020.

[16] A. E. Elmohlawy, V. F. Ochkov, and B. I. Kazandzhan, "Thermal performance analysis of a concentrated solar power system (CSP) integrated with natural gas combined cycle (NGCC) power plant," *Case Studies in Thermal Engineering*, vol. 14, article 100458, 2019.

[17] Y. Li and Y. Xiong, "Thermo-economic analysis of a novel cascade integrated solar combined cycle system," *Energy*, vol. 145, pp. 116–127, 2018.

[18] M. Amani, A. Smaili, and A. Ghenaiet, "A comparative study between two different techniques of solar integrated systems," *Applied Thermal Engineering*, vol. 211, article 118478, 2022.

[19] K. Ellingwood, K. Mohammadi, and K. Powell, "Dynamic optimization and economic evaluation of flexible heat integration in a hybrid concentrated solar power plant," *Applied Energy*, vol. 276, article 115513, 2020.

[20] K. Rashid, K. Mohammadi, and K. Powell, "Dynamic simulation and techno-economic analysis of a concentrated solar power (CSP) plant hybridized with both thermal energy storage and natural gas," *Journal of Cleaner Production*, vol. 248, article 119193, 2020.

[21] M. Petrollese and D. Cocco, "Techno-economic assessment of hybrid CSP-biogas power plants," *Renewable Energy*, vol. 155, pp. 420–431, 2020.

[22] R. Gutiérrez-Alvarez, K. Guerra, and P. Haro, "Market profitability of CSP-biomass hybrid power plants: towards a firm supply of renewable energy," *Applied Energy*, vol. 335, article 120754, 2023.

[23] P. G. Brodrick, A. R. Brandt, and L. J. Durlofsky, "Operational optimization of an integrated solar combined cycle under practical time-dependent constraints," *Energy*, vol. 141, pp. 1569–1584, 2017.

[24] N. Zhang, L. Duan, C. Huang et al., "Operation strategy and dynamic performance study of integrated solar combined-cycle system," *Energy Conversion and Management*, vol. 228, article 113716, 2021.

[25] A. L. K. Temraz, *Experimental and numerical investigation of the integrated solar combined cycle*, Technische Universität Darmstadt, Darmstadt, 2021.

[26] C. V. Ponce, D. Sáez, C. Bordons, and A. Núñez, "Dynamic simulator and model predictive control of an integrated solar combined cycle plant," *Energy*, vol. 109, pp. 974–986, 2016.

[27] F. Calise, M. D. d'Accadia, L. Libertini, and M. Vicidomini, "Thermoeconomic analysis of an integrated solar combined cycle power plant," *Energy Conversion and Management*, vol. 171, pp. 1038–1051, 2018.

[28] J. F. Servert, E. Cerrajero, D. López et al., "Base case analysis of a HYSOL power plant," *Energy Procedia*, vol. 69, pp. 1152–1159, 2015.

[29] J. García-Barberena, A. Monreal, A. Mutuberria, and M. Sánchez, "Towards cost-competitive solar towers - energy cost reductions based on decoupled solar combined cycles (DSCC)," *Energy Procedia*, vol. 49, pp. 1350–1360, 2014.

[30] A. Rovira, R. Abbas, C. Sánchez, and M. Muñoz, "Proposal and analysis of an integrated solar combined cycle with partial recuperation," *Energy*, vol. 198, article 117379, 2020.

[31] M. T. Islam, N. Huda, A. B. Abdullah, and R. Saidur, "A comprehensive review of state-of-the-art concentrating solar power (CSP) technologies: current status and research trends," *Renewable and Sustainable Energy Reviews*, vol. 91, pp. 987–1018, 2018.

[32] W. Wagner and A. Pruß, "The IAPWS formulation 1995 for the thermodynamic properties of ordinary water substance for general and scientific use," *Journal of Physical and Chemical Reference Data*, vol. 31, no. 2, pp. 387–535, 2002.

[33] D. R. Stull and H. Prophet, *JANAF Thermochemical Tables, Second Edition*, National Institute of Standards and Technology, Gaithersburg, MD, 1971.

[34] A. G. Fernández, H. Galleguillos, E. Fuentealba, and F. J. Pérez, "Thermal characterization of HITEC molten salt for energy storage in solar linear concentrated technology," *Journal of Thermal Analysis and Calorimetry*, vol. 122, no. 1, pp. 3–9, 2015.

[35] A. Rovira, *Data for the Paper: Towards High Solar Contribution in Hybrid CSP-Combined Cycle Gas Turbine Plants*, 2023.

[36] G. Ortega and A. Rovira, "A new method for the selection of candidates for shading and blocking in central receiver systems," *Renewable Energy*, vol. 152, pp. 961–973, 2020.

[37] G. Ortega and A. Rovira, "A fast and accurate methodology for the calculation of the shading and blocking efficiency in central receiver systems," *Renewable Energy*, vol. 154, pp. 58–70, 2020.

[38] R. Barbero, A. Rovira, M. J. Montes, and J. M. Martínez Val, "A new approach for the prediction of thermal efficiency in solar receivers," *Energy Conversion and Management*, vol. 123, pp. 498–511, 2016.

[39] A. Rovira, M. J. Montes, M. Valdes, and J. M. Martínez-Val, "Energy management in solar thermal power plants with double thermal storage system and subdivided solar field," *Applied Energy*, vol. 88, no. 11, pp. 4055–4066, 2011.

[40] G. Manente, "High performance integrated solar combined cycles with minimum modifications to the combined cycle power plant design," *Energy Conversion and Management*, vol. 111, pp. 186–197, 2016.

[41] A. M. El-Gammal, "An algorithm and criteria for compressor characteristics real time modeling and approximation," *Journal of Engineering for Gas Turbines and Power*, vol. 113, no. 1, pp. 112–118, 1991.

[42] A. Stamatis, K. Mathioudakis, and K. D. Papailiou, "Adaptive simulation of gas turbine performance," *Journal of Engineering for Gas Turbines and Power*, vol. 112, no. 2, pp. 168–175, 1990.

[43] P. P. Walsh and P. Fletcher, *Gas Turbine Performance*, Blackwell Science, Malden, MA, 2nd edition, 2004.

[44] "Typical Meteorological Year International Weather for Energy Calculation (TMY IWEC)," April 2023, https://bigladdersoftware.com/epx/docs/8-3/auxiliary-programs/source-weather-data-formats.html#:~:text=The%20IWEC%20data%20files%20are,U%20S%20National%20Climatic%20Data%20Center.

[45] A. Rovira, R. Abbas, M. Muñoz, and A. Sebastián, "Analysis of an integrated solar combined cycle with recuperative gas turbine and double recuperative and double expansion propane cycle," *Entropy*, vol. 22, no. 4, p. 476, 2020.

[46] A. Rovira, R. Barbero, M. J. Montes, R. Abbas, and F. Varela, "Analysis and comparison of integrated solar combined cycles using parabolic troughs and linear Fresnel reflectors as concentrating systems," *Applied Energy*, vol. 162, pp. 990–1000, 2016.

[47] Y. Li and Y. Yang, "Impacts of solar multiples on the performance of integrated solar combined cycle systems with two direct steam generation fields," *Applied Energy*, vol. 160, pp. 673–680, 2015.

[48] G. Manente, S. Rech, and A. Lazzaretto, "Optimum choice and placement of concentrating solar power technologies in integrated solar combined cycle systems," *Renewable Energy*, vol. 96, pp. 172–189, 2016.

[49] S. El Marazgioui and A. El Fadar, "Impact of cooling tower technology on performance and cost-effectiveness of CSP plants," *Energy Conversion and Management*, vol. 258, article 115448, 2022.

[50] H. Nezammahalleh, F. Farhadi, and M. Tanhaemami, "Conceptual design and techno-economic assessment of integrated solar combined cycle system with DSG technology," *Solar Energy*, vol. 84, no. 9, pp. 1696–1705, 2010.

[51] V. Zare, S. M. S. Mahmoudi, and M. Yari, "An exergoeconomic investigation of waste heat recovery from the gas turbine-modular helium reactor (GT-MHR) employing an ammonia-water power/cooling cycle," *Energy*, vol. 61, pp. 397–409, 2013.

[52] H. G. Kamath, R. Majumdar, A. V. Krishnan, and R. Srikanth, "Cost and environmental benefits of coal-concentrated solar power (CSP) hybridization in India," *Energy*, vol. 240, article 122805, 2022.